JACS
JOURNAL OF THE AMERICAN CHEMICAL SOCIETY
Communication
pubs.acs.org/JACS

General Strategy for Fabricating Thoroughly Mesoporous Nanofibers

Huilin Hou,[†,‡] Lin Wang,[†] Fengmei Gao,[†] Guodong Wei,[†] Bin Tang,[‡] Weiyou Yang,*[,†] and Tom Wu*[,§]

[†]Institute of Materials, Ningbo University of Technology, Ningbo 315016, P. R. China

[‡]Research Institute of Surface Engineering, Taiyuan University of Technology, Taiyuan 030024, P. R. China

[§]Materials Science and Engineering, King Abdullah University of Science and Technology (KAUST), Thuwal 23955-6900, Saudi Arabia

Supporting Information

ABSTRACT: Recently, preparation of mesoporous fibers has attracted extensive attentions because of their unique and broad applications in photocatalysis, optoelectronics, and biomaterials. However, it remains a great challenge to fabricate thoroughly mesoporous nanofibers with high purity and uniformity. Here, we report a general, simple and cost-effective strategy, namely, foaming-assisted electrospinning, for producing mesoporous nanofibers with high purity and enhanced specific surface areas. As a proof of concept, the as-fabricated mesoporous TiO_2 fibers exhibit much higher photocatalytic activity and stability than both the conventional solid counterparts and the commercially available P25. The abundant vapors released from the introduced foaming agents are responsible for the creation of pores with uniform spatial distribution in the spun precursor fibers. The present work represents a critically important step in advancing the electrospinning technique for generating mesoporous fibers in a facile and universal manner.

Mesoporous materials are of great interest in the fields of catalysis, selective adsorption, and host/guest supports, owing to their high specific surface areas as compared to their conventional solid counterparts.[1] Recently, preparation of mesoporous micro/nanofibers has particularly attracted extensive attentions because of their broad applications in photocatalysis, optoelectronics, and biomaterials.[2] Besides the intrinsic porous characteristics, the one dimensional (1D) mesoporous nanofibers provide efficient paths for the electron transportation and possess a robust geometry to maintain the functionalities.[3] Up to date, several methods have been invented to fabricate mesoporous nanofibers, such as hydrothermal route,[4] template-assisted process,[5] electrospinning technique,[6] structure-selective synthesis,[7] and so on. However, it still remains a great challenge to fabricate thoroughly mesoporous nanofibers with satisfied purity and uniformity in a simple and universal manner.

Electrospinning is a versatile, simple, and cost-effective strategy for producing 1D nanostructures of a wide range of materials with tunable diameters and morphologies.[8] However, most of the reported works were focused on the fabrication of conventional solid fibers without any pores. Can we advance the facile technique of electrospinning to create mesoporous fiber structures? Such a breakthrough will lead to the fabrication of mesoporous fibers with enhanced specific surface areas in a controlled manner. This is the primary motivation behind the present work. Here, we report a general strategy, namely, foaming-assisted electrospinning, for the synthesis of mesoporous fibers. TiO_2 and TiO_2-based composites are chosen as the examples to demonstrate the versatile and general nature of our approach. The resultant mesoporous fibers exhibit much better performance compared to the conventional nanofibers and the commercially available P25 product, suggesting their very promising application prospect. The present work might open new doors for the exploration of mesoporous nanofibers with high photocatalytic activities.

TiO_2 mesoporous nanofibers were fabricated by calcination of precursor fibers, which were obtained by electronspinning the solution of polyvinylpyrrolidone (PVP), tetrabutyl titanate (TBOT), and foaming agent diisopropyl azodiformate (DIPA). The raw materials of TBOT (Aladdin, Shanghai, China), PVP (MW ≈ 1300000, Aladdin, Shanghai, China) and DIPA (Adamas, Shanghai, China) were commercially available and directly used without further purification. Absolute ethyl alcohols and acetic acid were used as the solvents to homogeneously mix TBOT, PVP, and DIPA. In a typical experiment, PVP, TBOT, and solvents were first mixed by vigorously stirring for 6 h. PVP is used here to tune the viscosity of the solution. DIPA of 10 wt % was then added into the above solution with further magnetic stirring for 2 h. The resultant solution was transferred into a plastic syringe with a stainless steel nozzle (anode, diameter 0.22 mm). The tip of the stainless steel nozzle was placed in the front of a metal cathode (collector) with a typically fixed distance of 20 cm between the nozzle and the collector. An electrical potential of 18 kV was applied for electrospinning the precursor fibers, and then the products were dried in oven at 60 °C. Subsequently, the precursor fibers were positioned in a quartz crucible and annealed in a tube furnace at 550 °C in air for 2 h, before cooling to the ambient temperature. For comparison, a control experiment was also carried out without the foaming agent addition in the initial solutions, and the details are shown in Table S1 (Supporting Information, SI). The resultant products were referred as Samples A1 and A2, respectively. To show the universality of this technique for generating mesoporous fibers, TiO_2-based hybrid mesoporous nanofibers were also synthesized with the similar experimental procedures. Zinc acetate ($Zn(Ac)_2$), copper acetate ($Cu(Ac)_2$), and ferric acetylacetonate (Fe AcAc) were used as the raw materials in the synthesis of TiO_2/

Received: August 27, 2014
Published: November 18, 2014

dx.doi.org/10.1021/ja508840c | J. Am. Chem. Soc. 2014, 136, 16716−16719

$ZnTiO_3$, TiO_2/CuO, and TiO_2/Fe_2O_3 hybrid nanofibers, respectively. Dimethylformamide (DMF) was added to improve the solubility of precursors during the preparation of the solutions. The detailed compositions of the initial solutions are shown in Table S2 (SI), and the resultant products were referred as Samples B–D, respectively. The details for structure characterization and photocatalytic performance measurement of the mesoporous fibers are shown in the SI.

Scanning electron microscopy (SEM) was employed to characterize the spun precursor fibers and their corresponding calcined products. The as-spun precursor fibers of Sample A1 have smooth surfaces with average diameter of ~1 μm and lengths up to several hundred of millimeters. The corresponding elemental mappings show uniform spatial distribution of Ti, N, and O (Figure S1, SI). Figure 1a shows the typical SEM images of the calcined fibers (also see Figure S2a–c, SI). All the precursor nanofibers have been completely converted into mesoporous nanofibers with a high purity. The fiber diameter is reduced to ~600 nm, mainly owing to the elimination of PVP and the formation of crystalline TiO_2 after the high-temperature treatment. Figure 1b shows a representative cross-section SEM image of the TiO_2 mesoporous nanofibers, disclosing that the fibers possess a thoroughly porous structure with homogeneous pores.

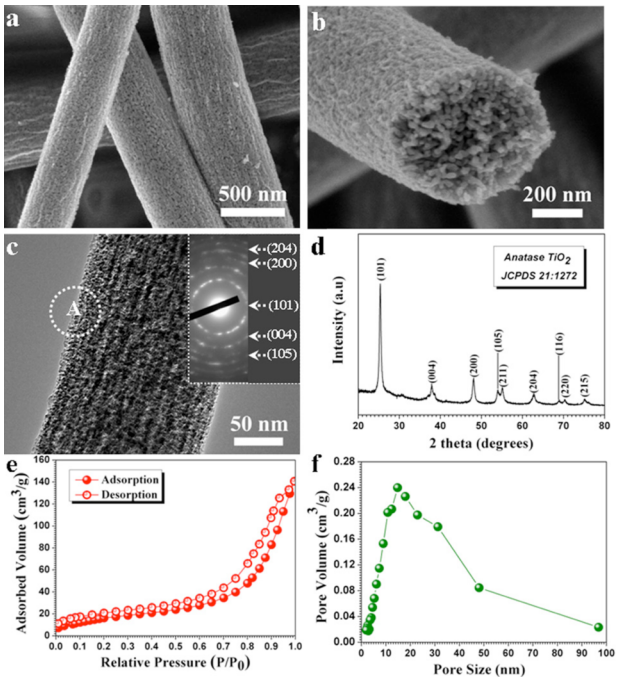

Figure 1. (a,b) Typical SEM images of the TiO_2 mesoporous nanofibers under different magnifications. (c) A representative TEM image of a single mesoporous TiO_2 nanofiber. The inset is the corresponding SAED pattern recorded from the marked area of A in panel c. (d) A typical XRD pattern of Sample A1 after calcination. (e) Nitrogen adsorption–desorption isotherm of the TiO_2 mesoporous nanofibers. (f) Corresponding pore size distribution.

Figure 1c provides a representative TEM image of a single TiO_2 nanofiber, further confirming that densely distributed pores exist throughout the fiber body. The SAED pattern (the inset in Figure 1c) recorded at the marked area in Figure 1c suggests that the obtained product is anatase TiO_2 (JCPDS, No. 21-1272) with a polycrystalline nature. Furthermore, the EDS spectrum discloses that the fibers possess only Ti and O (Figure S2d, SI). Although the DIPA foamer contains N, we did not detect any N in the calcined fibers. We should also mention that many long mesoporous fibers survived the scratching and ultrasonic treatments during the TEM sample preparation process, indicating their high structural robustness. Figure 1d presents the typical XRD pattern of the calcined products of Sample A1. All the peaks can be indexed to the anatase TiO_2 (JCPDS, No. 21-1272), suggesting the pure phase of the resultant fibers. The sharp diffraction peaks indicate that the products are highly crystalline.

Nitrogen adsorption measurements (Figure 1e) revealed that the products exhibit the type IV isotherm behavior with H3 hysteresis, implying that the obtained fibers are mesoporous with a Brunauer–Emmett –Teller (BET) surface area of ~64.9 m^2/g. The distribution of Barrett–Joyner–Halenda (BJH) pore sizes (Figure 1f) determined from the adsorption branches are peaked at ~16 nm.

A control experiment without the foaming agent added in the initial solutions (see Sample A2 in Table S1, SI) was carried out to isolate the effect of the foaming agent of DIPA on the formation of the porous fibers. The as-spun polymer fibers are similar to those of Sample A1 (Figure S3a,b, SI). However, their calcined products present the ordinary solid nanofibers (Figure S3c,d, SI), which are quite different from the mesoporous structures synthesized with the 10 wt % foaming agents, suggesting that the introduced foaming agents are critical for the formation of the mesoporous structures. The XRD pattern (Figure S3e, SI) discloses that the as-prepared Sample A2 is also pure anatase TiO_2, implying that the foaming agent has no effect on the compositions of the resultant products. However, the calcined fibers of Sample A2 shows a BET surface area of ca. 11.9 m^2/g (Figure S3f, SI), which is about 6 times lower than that of Sample A1 (64.9 m^2/g). Table S3 in the SI summarizes the surface properties of the Samples A1 and A2. Sample A1 possesses much higher pore volume than A2, implying that the foaming agent of DIPA is responsible for the formation of the mesopores within the fibers. This comparison unambiguously suggests (i) the foaming agents play a critically important role on the formation of the mesoporous fibers, which helps create the pores throughout the entire body of fibers with uniform spatial distribution and (ii) the foaming agents significantly enhance the BET surface area of the resultant fibers.

The formation mechanism of the mesoporous fibers could be explained as follows (schematically shown in Figure S4a, SI). First, the DIPA, the foaming agent, is assembled into the precursor fibers (Step I). Since the DIPA is dissolved in the solutions before electrospinning, the foamer is distributed homogeneously within the fibers. The homogeneous distribution of DIPA is consistent with elemental mapping data and the formation of uniform porous structure throughout the fiber body. During the calcination process under air at 550 °C (Step II), the DIPA foamer, with the chemical formula of $C_8H_{14}N_2O_4$, is completely decomposed into vapor phases (e.g., CO_2, NO_2, and H_2O), which cause the formation of the pores within the fibers. This is confirmed by the thermal analysis of the as-spun PVP/TBOT/DIPA fibers of Sample A1 (Figure S4b, SI). The initial slight weight loss in the low temperature range (35–130 °C) is owing to the residual solvent decomposition and volatilization. The 10% weight loss between 130 and 180 °C is caused by the decomposition of DIPA (DSC exdothermic peak at ~160 °C), which results in the formation of mesoporous precursor nanofibers. The 40% weight loss at the higher temperatures (300–480 °C) should be attributed to the

dx.doi.org/10.1021/ja508840c | J. Am. Chem. Soc. 2014, 136, 16716–16719

decomposition of PVP (DSC endothermic peak at 420 °C). Finally, the DSC exdothermic peak at 500 °C is attributed to the TiO_2 crystallization. In contrast, as shown in Figure S4b (SI), there are only two exothermic peaks observed for Sample A2, which are related to PVP decomposition and TiO_2 crystallization. These data suggest that the introduction of the DIPA foaming agents notably affects the thermal behaviors of as-spun fibers.

The as-fabricated TiO_2 mesoporous nanofibers (Sample A1) and solid TiO_2 nanofibers (Sample A2), as well as the commercial P25, were used as the photocatalysts for evaluation of their photocatalytic properties. The surface properties of P25 are shown in Table S3, SI. Figure 2a plots the evolution of

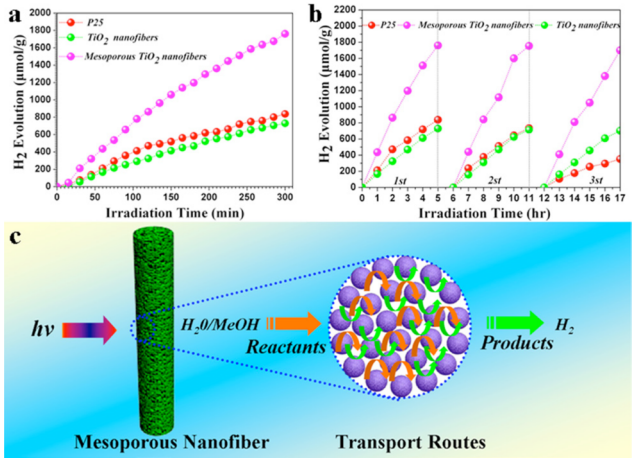

Figure 2. (a) Hydrogen production photocatalyzed by the as-fabricated mesoporous TiO_2 nanofibers, solid TiO_2 nanofibers, and P25 under different irradiation time. (b) Results of reusability experiments for photocatalytic H_2 generation using the present three photocatalysts. (c) Schematic illustration of mesoporous fibers with enhanced photocatalytic activities.

hydrogen produced from the aqueous suspensions of the three photocatalysts (their average hydrogen production rates are shown in Figure S5, SI). It is clear that the hydrogen evolution rate of the TiO_2 mesoporous nanofibers (ca. 399.2 μmol g^{-1} h^{-1}) is much higher than those of solid counterpart (ca. 156.9 μmol g^{-1} h^{-1}) and P25 (ca. 197.8 μmol g^{-1} h^{-1}), suggesting that the creation of pores in/on the fibers by the foaming agents significantly improves the photocatalytic activity of TiO_2. More interestingly, the hydrogen production rate of thoroughly mesoporous TiO_2 nanofibers is higher than most values reported for solid and porous TiO_2 nanofibers (see Table S4, SI). To further investigate their reusability and stability, these three photocatalysts were recovered and reused for photocatalytic H_2 production under the similar conditions. As shown in Figure 3b, there is nearly no loss of H_2 evolution rate for both mesoporous and solid TiO_2 fiber photocatalysts, whereas the activity of P25 evidently declined after 3 cycles. This confirms that the obtained mesoporous TiO_2 fibers are much more stable with a higher photocatalytic activity than the commercial product of P25. To account for the high performance of mesoporous TiO_2 fibers, a schematic diagram is illustrated in Figure 3c. First, the one-dimensional (1D) fibers could remarkably inhibit the agglomeration of nanoparticles, which contributes to the stable photocatalytic performance.[9] Second, the columnar mesoporous architecture possesses the interconnected channels, which offers more active sites to adsorb reactants, e.g., water and MeOH

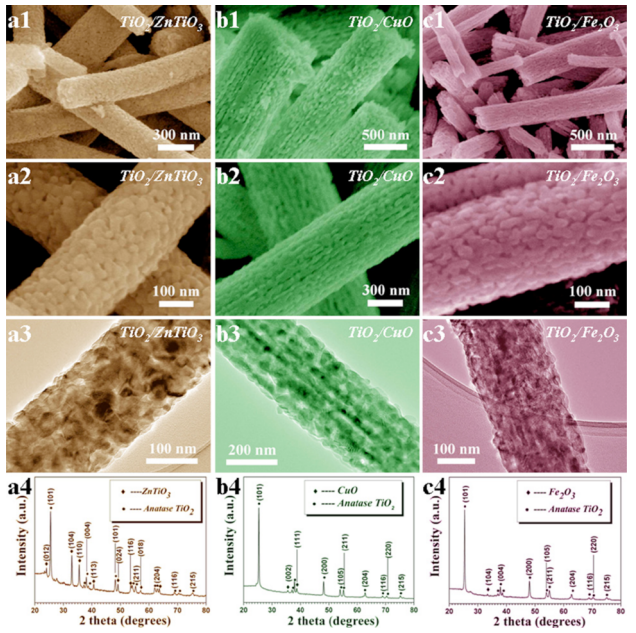

Figure 3. (a1–c2) Typical SEM images of the hybrid mesoporous nanofibers of $TiO_2/ZnTiO_3$ (a1–a2), TiO_2/CuO (b1–b2), and TiO_2/Fe_2O_3 (c1–c2). (a3–c3) Typical TEM images of individual mesoporous nanofibers from Samples B, C, and D, respectively. (a4–c4) Representative XRD patterns recorded from the calcined products of Samples B, C, and D.

groups. Finally, the mesoporous channels existing throughout the fibers allow the effective transportation of gaseous products.[10] In other words, the morphology of the 1D mesoporous fibers is beneficial to the participation materials moving easily into/out of the framework, yielding a high reaction rate. These synergetic effects as mentioned above are responsible for the much improved photocatalytic properties of the mesoporous fibers with high activity and stability.

Now we come to the point on the versatile and universal characteristics of the present foaming-assisted electrospinning technique for producing mesoporous nanofibers. Three TiO_2-based hybrid materials are chosen as the examples (see Table S2, SI). Figure 3a1–c2 displays the representative SEM images of the calcination products corresponding to the as-spun precursor fibers of Samples B, C, and D (i.e., using zinc acetate, copper acetate, and ferric acetylacetonate as the precursors, respectively) (Figure S6, SI), suggesting that the precursor fibers have been completely converted to mesoporous fibers (Figure S7, SI). Close observations on the cross sections (Figure S7, SI) indicate that all the fibers are thoroughly mesoporous. Figure 3a3–c3 depicts the typical TEM images of Samples B, C, and D, respectively, further confirming their thoroughly mesoporous nature (also see Figures S8a–S10a, SI). Figure 3a4–c4 displays the typical XRD patterns corresponding to Samples B, C, and D. These experimental results suggest that the obtained three samples are $TiO_2/ZnTiO_3$, TiO_2/CuO, and TiO_2/Fe_2O_3 hybrid fibers, respectively, which are consistent with the SAED analyses (Figures S8b–S10b, SI). The EDS analyses (Figures S8c–S10c, SI) disclose the presence of Zn, Cu, and Fe elements, respectively, besides Ti and O, consistent with the expected compositions. The HRTEM images (Figure S8d–f–S10d–f, SI) further confirm that the synthesis products are $TiO_2/ZnTiO_3$, TiO_2/CuO, and TiO_2/Fe_2O_3 hybrid fibers. The results of BET surface areas and the pore size distribution measurements

dx.doi.org/10.1021/ja508840c | J. Am. Chem. Soc. 2014, 136, 16716–16719

(Figure S11, SI) indicate that these three products also display the type IV-like isotherm with H3 hysteresis, and the BET surface areas are ~37.8, 50.7, and 35.9 m^2/g for $TiO_2/ZnTiO_3$, TiO_2/CuO, and TiO_2/Fe_2O_3 hybrid fibers with average pore sizes of 17.1, 16.2, and 38.3 nm, respectively. The surface properties of the three hybrid products are summarized in Table S5, SI. These results demonstrate that diverse materials can be fabricated simply by using the corresponding raw materials, suggesting the versatility and universality of the present foaming-assisted electrospinning technique for the fabrication of mesoporous fibers.

In summary, we have demonstrated a novel and general strategy, namely, foaming-assisted electrospinning, for producing mesoporous nanofibers. This universal method is effective for generating thoroughly mesoporous fibers with high purity and remarkably enhanced specific surface areas. As a proof of concept, the as-fabricated mesoporous TiO_2 fibers exhibit a much higher photocatalytic activity and stability than both the conventional solid counterparts and the commercially available P25. The release of vapor phases from the introduced foaming agents is responsible for the creation of pores in/on the polymeric precursor fibers, leading to the formation of mesoporous structures. Our work opens new doors for the exploration of thoroughly mesoporous fibers, and the novel synthesis will advance such materials toward the high-performance applications as photocatlysts and catalyst supports.

■ ASSOCIATED CONTENT

Supporting Information

Experimental procedures, additional data including SEM, TEM, XRD, TG-DCS, and BET of the example products, and schematic illustration for the formation of mesoporous nanofibers. This material is available free of charge via the Internet at http://pubs.acs.org.

■ AUTHOR INFORMATION

Corresponding Authors

*weiyouyang@tsinghua.org.cn
*tao.wu@kaust.edu.sa

Notes

The authors declare no competing financial interest.

■ ACKNOWLEDGMENTS

This work was supported by the 973 program (Grant No. 2012CB326407), National Natural Science Foundation of China (NSFC, Grant Nos. 51372122 and 51372123), and Outstanding Innovation Project for Graduate Student in Shanxi Province (Grant No. 20133040). This work was also supported by King Abdullah University of Science and Technology (KAUST).

■ REFERENCES

(1) (a) Zhao, D.; Feng, J.; Huo, Q.; Melosh, N.; Fredrickson, G. H.; Chmelka, B. F.; Stucky, G. D. *Science* **1998**, *279*, 548. (b) Zou, X.; Conradsson, T.; Klingstedt, M.; Dadachov, M. S.; O'Keeffe, M. *Nature* **2005**, *437*, 716. (c) Li, H.; Bian, Z.; Zhu, J.; Zhang, D.; Li, G.; Huo, Y.; Li, H.; Lu, Y. *J. Am. Chem. Soc.* **2007**, *129*, 8406. (d) Warren, S. C.; Messina, L. C.; Slaughter, L. S.; Kamperman, M.; Zhou, Q.; Gruner, S. M.; DiSalvo, F. J.; Wiesner, U. *Science* **2008**, *320*, 1748. (e) Wu, Z.; Wu, W. D.; Liu, W.; Selomulya, C.; Chen, X. D.; Zhao, D. *Angew. Chem., Int. Ed.* **2013**, *52*, 13764.

(2) (a) Huo, Q.; Zhao, D.; Feng, J.; Weston, K.; Buratto, S. K.; Stucky, G. D.; Schacht, S.; Schüth, F. *Adv. Mater.* **1997**, *9*, 974. (b) Zhan, S.; Chen, D.; Jiao, X.; Song, Y. *Chem. Commun.* **2007**, *20*, 2043. (c) Hong, Y.; Chen, X.; Jing, X.; Fan, H.; Gu, Z.; Zhang, X. *Adv. Funct. Mater.* **2010**, *20*, 1503. (d) Mao, C.; Wang, F.; Cao, B. *Angew. Chem., Int. Ed.* **2012**, *124*, 6517.

(3) (a) Wang, K.; Wang, Y.; Wang, Y.; Hosono, E.; Zhou, H. *J. Phys. Chem. C* **2008**, *113*, 1093. (b) Lee, K. J.; Min, S. H.; Jang, J. *Chem. Eur. J.* **2009**, *15*, 2491. (c) Liu, H. J.; Wang, X. M.; Cui, W. J.; Dou, Y. Q.; Zhao, D. Y.; Xia, Y. Y. *J. Mater. Chem.* **2010**, *20*, 4223.

(4) (a) Bavykin, D. V.; Parmon, V. N.; Lapkin, A. A.; Walsh, F. C. *J. Mater. Chem.* **2004**, *14*, 3370. (b) Yang, Y.; Suzuki, M.; Fukui, H.; Shirai, H.; Hanabusa, K. *Chem. Mater.* **2006**, *18*, 1324.

(5) (a) Yang, Z.; Niu, Z.; Cao, X.; Yang, Z.; Lu, Y.; Hu, Z.; Han, C. C. *Angew. Chem., Int. Ed.* **2003**, *42*, 4201. (b) Chae, W. S.; Lee, S. W.; Kim, Y. R. *Chem. Mater.* **2005**, *17*, 3072.

(6) (a) Zhan, S.; Chen, D.; Jiao, X.; Tao, C. *J. Phys. Chem. B* **2006**, *110*, 11199. (b) Zhang, W.; Zhu, R.; Ke, L.; Liu, X.; Liu, B.; Ramakrishna, S. *Small* **2010**, *6*, 2176. (c) Saha, J.; De, G. *Chem. Commun.* **2013**, *49*, 6322.

(7) (a) Wang, J.; Zhang, J.; Asoo, B. Y.; Stucky, G. D. *J. Am. Chem. Soc.* **2003**, *125*, 13966. (b) Wang, J.; Tsung, C. K.; Hong, W.; Wu, Y.; Tang, J.; Stucky, G. D. *Chem. Mater.* **2004**, *16*, 5169.

(8) (a) Li, D.; Wang, Y.; Xia, Y. *Nano Lett.* **2003**, *3*, 1167. (b) McCann, J. T.; Marquez, M.; Xia, Y. *J. Am. Chem. Soc.* **2006**, *128*, 1436. (c) Greiner, A.; Wendorff, J. H. *Angew. Chem., Int. Ed.* **2007**, *46*, 5670. (d) Zhu, C.; Yu, Y.; Gu, L.; Weichert, K.; Maier, J. *Angew. Chem., Int. Ed.* **2011**, *50*, 6278. (e) Inagaki, M.; Yang, Y.; Kang, F. *Adv. Mater.* **2012**, *24*, 2547. (f) Nandakumar, A.; Truckenmüller, R.; Ahmed, M.; Damanik, F.; Santos, D. R.; Auffermann, N.; de Boer, J.; Habibovic, P.; van Blitterswijk, C.; Moroni, L. *Small* **2013**, *9*, 3544.

(9) (a) Bao, N.; Shen, L.; Takata, T.; Domen, K. *Chem. Mater.* **2007**, *20*, 110. (b) Wu, H. B.; Hng, H. H.; Lou, X. W. D. *Adv. Mater.* **2012**, *24*, 2567.

(10) (a) Yu, J. C.; Wang, X.; Fu, X. *Chem. Mater.* **2004**, *16*, 1523. (b) Guo, C.; Ge, M.; Liu, L.; Gao, G.; Feng, Y.; Wang, Y. *Environ. Sci. Technol.* **2009**, *44*, 419. (c) Zhou, W.; Li, W.; Wang, J.; Qu, Y.; Yang, Y.; Xie, Y.; Zhang, K.; Wang, L.; Fu, H.; Zhao, D. *J. Am. Chem. Soc.* **2014**, *136*, 9280.